Topographic Waves Generated by a Transient Wind

FRANÇOIS LOTT* AND HECTOR TEITELBAUM

Laboratoire de Météorologie Dynamique du C.N.R.S., Ecole Polytechnique, Palaiseau, France

(Manuscript received 16 December 1991, in final form 24 August 1992)

ABSTRACT

The concept of linear mountain waves is generally equated with steady-state stationary waves. This essentially means that the absolute horizontal phase velocity of mountain waves is zero and that their momentum flux profile is independent of height and time in the absence of dissipation and zero-level wind. This paper investigates the generation of linear unsteady mountain gravity waves. The incident flow is transient, starting from zero at a given time and returning to zero after a finite time. The topography is a single horizontal harmonic. The unsteadiness of the waves is due partly to the temporal change of their phase velocity, which takes place during their propagation in the time-dependent mean flow. When the wind ceases, most of the waves present have a phase velocity nearly opposite to the maximum wind. For this reason, mountain waves can propagate through levels of zero mean wind. The transient structure of the wave field also comes from the temporal change of the amplitude of the ground forcing. Moreover, it is the result of the interference between the waves generated while the wind increases and those generated while it decreases. These transient effects naturally lead to z-dependent momentum flux profiles that are analyzed in detail.

This paper deals with an analytical model, when the unsteady incident flow is uniform in the vertical direction. When the incident wind varies slowly in time, a comprehensive picture of the wave field is given by an asymptotic expansion of the wave solution. When the mean flow changes rapidly in time and when it varies in the vertical direction, the solution is obtained with a numerical model.

1. Introduction

The atmospheric waves generated over a bottom topography whose horizontal scale is small enough to neglect the earth rotation have been studied by many authors. The first comprehensive treatment of these waves was made in the linear case by Queney (1947) and Scorer (1949). It has been extended to finite amplitude topography by Long (1953). Thereafter, linear and nonlinear studies have been developed in order to give a comprehensive picture of these waves and of the associated severe downslope windstorms occurring in the lee of mountains (Peltier and Clark 1979; Durran 1986; Durran and Klemp 1987; Klemp and Lilly 1975; Bacmeister and Pierrehumbert 1988). In general, these studies assume that the incident flow is steady, although some unsteadiness in the wave field is expected at the start of the incident flow (Palm 1953; Jusem and Barcilon 1985). In other studies, unsteadiness results from local instabilities of the main wave (Laprise and Peltier 1989; Bacmeister and Schoeberl 1989). In all of these studies, most of the energy of the disturbance is transported by a main stationary wave, because the incident flow becomes steady after a finite time.

Observations show that this assumption is not always valid. Some atmospheric examples can be found in Smith (1982), who shows synoptic observations of wind and pressure near a mountain. In this case, the time-dependent component of the incident flow is related to the passage of synoptic disturbances. More common geophysical examples of transient flow interaction with mountains have been studied by oceanographers (Bell 1975) in the context of the interaction between the fluctuating tides and the bottom topography. In this context, the mean flow varies as a single harmonic in time, allowing certain simplifications in the mathematical treatment of the problem. Nevertheless, in the atmospheric case, this temporal structure of the incident flow is not relevant, the amplitude of the atmospheric tides being small in the troposphere compared to that of the synoptic disturbances. To approach the atmospheric context, Bannon and Zehnder (1985) added a steady component to such a sinusoidally varying flow. They studied the influence of transience on the mountain drag, including the effect of the Coriolis force. They found that some evanescent long modes, which do not participate in the mountain drag in the steady case (Smith 1979), can contribute to the instantaneous mountain drag in the unsteady case. In this paper, we investigate situations where the time-varying wind is not a single temporal harmonic.

* Current affiliation: European Centre for Medium-Range Weather Forecasts, Reading, Berkshire, England.

Corresponding author address: Dr. Francois Lott, European Centre for Medium-Range Weather Forecasts, Shinfield Park, Reading, Berkshire, England, RG29AX.

In order to provide a simple description of transient mountain waves, we study cases for which the incident wind has at most one increasing phase and one decreasing phase. It is very different from the case of a sinusoidally varying wind where an infinite number of increases and decreases of the incident wind contribute to the wave field. It is supposed to idealize the time behavior of winds in realistic situations, such as the interaction between a front and a topography.

The nature of transient effects on topographically disturbed flow depends on the relative size of the time scale, $\tilde{t}_f$, that characterizes the temporal fluctuations of the incident flow and of the time, $\tilde{t}_a$, required for the formation of the wave pattern over one vertical wavelength:

$$\tilde{t}_a \approx (\tilde{C}_{gz}\tilde{m})^{-1} \approx (\tilde{k}U_0)^{-1}.$$

Here, $\tilde{k}$ and $\tilde{m}$ are the horizontal and vertical wavenumbers of the disturbance, U_0 is the maximum wind amplitude, $\tilde{C}_{gz}$ is a characteristic vertical group velocity of the wave,

$$\tilde{C}_{gz} \approx \frac{\tilde{k}U_0^2}{N},$$

and N is the buoyancy frequency. The tilde symbol is used to identify dimensional variables. The time scale, $\tilde{t}_a$, is also the advective time required for a fluid particle to cover one wavelength of the mountain range. The case, $\tilde{t}_f \ll \tilde{t}_a$, reduces essentially to a ground-generated vibrating disturbance in a stationary fluid. It was studied by Chimonas (1977) in order to explain the observation of infrasounds in the vicinity of mountains. The situations for which $\tilde{t}_f \gg \tilde{t}_a$ are called quasi steady. In these cases, the importance of the time variation of the mean flow on the wave depends on the relative size of the time scale, $\tilde{t}_f$, and of the scale,

$$\tilde{t}_w = L/\tilde{C}_{gz},$$

which characterizes the time required for the waves to traverse a layer of height L, where temporal variation of the mean flow occurs. For values characterizing the tropopause (L = 10 km, N = 0.01, U_0 = 10 m s^{-1}), $\tilde{t}_w$, is greater than one hour as soon as the horizontal wavenumber ($\tilde{\lambda}_x$) of the wave exceeds 20 km. Consequently, in the troposphere, the structure of mountain gravity waves can be significantly affected by the temporal variations of the flow occurring over one hour. For middle atmosphere dynamics ($L \approx 80$ km, $N \approx 0.02$), $\tilde{t}_w$ is longer than 1 day as soon as $\tilde{\lambda}_x > 30$ km. Therefore, we should take into account the influence on these waves of the mean flow fluctuations, induced by the planetary waves of short period.

For a quasi-steady flow, the temporal change of the incident wind induces temporal variation of wave amplitudes at the ground. This naturally gives rise to a transient wave field of which the momentum flux profile varies with height. It gives rise to mean flow changes (Eliassen and Palm 1960; Andrews and McIntyre 1976) in spite of the fact that the fluid is not viscous.

Furthermore, in quasi-steady flows, a direct effect of the mean flow temporal change on a wave is to modify its frequency (Lighthill 1978). Thus, the topographic waves, which have zero phase velocity when they are generated on the mountain, will have nonzero phase velocity when the wind stops. In this case, the topographic waves do not encounter critical levels where the mean wind falls to zero. This is contrary to the result of Eliassen and Palm (1960), who have studied topographic waves in a steady flow. For these reasons, unsteady topographic waves can propagate up to higher levels than steady waves. They can also encounter critical levels where the mean wind is not zero. In any case, the gravity wave critical-level interaction is an important process of the atmospheric dynamics. When a gravity wave reaches a critical level, complex wave–mean flow interactions occur. Assuming that the mean Richardson number is generally larger than 0.25, the wave is absorbed and deposits its momentum at the critical level (Booker and Bretherton 1967). This result is valid for small amplitude waves at large Reynolds number (Lott and Teitelbaum 1990). For large amplitude waves, the critical-level interaction is nonlinear, and the reflection of the wave can be large while its transmission remains very small (Brown and Stewartson 1980). For unstable flows, the dynamics of the gravity wave critical-level interaction resembles that of instability (Jones 1968; Lindzen and Rosenthal 1983; Lindzen and Rambaldi 1986; Lindzen and Tung 1978). If the waves do not reach critical levels, they attain altitudes where they restore momentum to the mean flow through viscous processes or wave breaking (Lindzen 1981; Schoeberl 1988).

The purpose of the present study is to investigate the structure of the gravity waves generated by transient wind incident over a single harmonic mountain range. The incident wind starts from zero at a given moment, reaching its maximum amplitude after a finite time and returning to zero thereafter. In the second section of this study, we consider a wind profile that is constant in the vertical direction. An analytical solution is obtained and an asymptotic expansion of the wave field is given when the time fluctuations of the mean wind are slow (or quasi steady). This helps to develop some physical insight into the dynamics of topographic waves, generated by a time-varying incident flow. In the third section, a numerical model is used. It allows us to validate the preceding analytical calculations and to extend them to more rapid winds. Furthermore, particular attention is paid to the mean flow acceleration induced by wave transience. For this purpose, the momentum fluxes obtained for different temporal profiles of the incident wind (including the case for which the incident wind reaches a constant value) are compared. They are also compared to the momentum flux profile induced by a transient gravity wave whose

amplitude variation is forced at the ground when the phase velocity is nearly constant. This kind of model has been used by Dunkerton (1981) and Fritts and Dunkerton (1984) to study transient gravity waves. We also examine the case for which the unsteady wind is always zero at a given height. We determine whether topographic waves can propagate vertically through such a level, which is a critical level for topographic waves in steady flow.

2. Uniform mean flow in the vertical direction

a. General solution

We modify the well-known Queney (1947) problem to allow the spatially uniform incident wind to be a function of time. The model atmosphere is a stratified, inviscid, hydrostatic, and Boussinesq fluid. The use of the Boussinesq approximation deserves comment. In fact, in this approximation, the influence of the background fluid compressibility on the waves is neglected. Consequently, the exponential growth of gravity waves with height, which leads to gravity wave breaking in the high atmosphere, is not represented. Nevertheless, we assume that the characteristic vertical wavenumber of the mountain waves, N/U_0, is large compared to the inverse of the density scale height, g/RT_0. Then, the mean flow compressibility has a weak influence on the horizontal and vertical group velocities of the waves. For this reason, we can adopt the Boussinesq approximation, since we study the characteristics of mountain wave propagation rather than their breaking. Although the Coriolis force is important for the case of long mountains in the unsteady case (Bannon and Zehnder 1985), we further assume that the characteristic intrinsic frequency of the waves considered is large as compared to the Coriolis parameter (i.e., the Rossby number is large) and we do not take into account the effect of the earth rotation.

The basic-state velocity field is a zonal wind of the form:

$$\tilde{u}_0(\tilde{t}) = U_0 U(\tilde{t}).$$

This flow is incident on a corrugated mountain, the profile of which is given by

$$\tilde{h}(\tilde{x}) = \mathrm{Re}[H_0 \exp(+i\tilde{k}\tilde{x})].$$

Here H_0 is the maximum mountain height and $\tilde{k}$ its horizontal wavenumber. The mountain is assumed to force a small linear perturbation into the basic flow. This is known to be true when the characteristic vertical wavenumber of the disturbance is large compared to the mountain height. It corresponds to a situation of small inverse Froude number:

$$\mathrm{Fr}^{-1} = \frac{NH_0}{U_0} \ll 1.$$

Here, N is the constant buoyancy frequency associated with the stable basic-state density stratification ρ_0:

$$N^2 = -g\frac{1}{\rho_0}\frac{d\rho_0}{d\tilde{z}}.$$

Writing all the wave field parameters as:

$$\tilde{f}_1(\tilde{t}, \tilde{x}, \tilde{z}) = \mathrm{Re}[\hat{f}_1(\tilde{t}, \tilde{z}) \exp(i\tilde{k}\tilde{x})],$$

the disturbed flow satisfies the equations:

$$\left(\frac{\partial}{\partial \tilde{t}} + i\tilde{k}\tilde{u}_0(\tilde{t})\right)\hat{u}_1 + i\tilde{k}\frac{\hat{p}_1}{\rho_0} = 0 \tag{2.1}$$

$$\frac{\partial \hat{p}_1}{\partial \tilde{z}} + g\hat{\rho}_1 = 0 \tag{2.2}$$

$$\left(\frac{\partial}{\partial \tilde{t}} + i\tilde{k}\tilde{u}_0(\tilde{t})\right)\frac{\hat{\rho}_1}{\rho_0} - \frac{N^2}{g}\hat{w}_1 = 0 \tag{2.3}$$

$$i\tilde{k}\hat{u}_1 + \frac{\partial \hat{w}_1}{\partial \tilde{z}} = 0. \tag{2.4}$$

Here, $\hat{p}_1$ and $\hat{\rho}_1$ are the pressure and density perturbations. The kinematic boundary condition at the surface is

$$\hat{w}_1(\tilde{t}, \tilde{z} = 0) = i\tilde{k}\tilde{u}_0(\tilde{t})H_0. \tag{2.5}$$

Introducing U_0, $\tilde{k}^{-1}$, $(\tilde{k}U_0)^{-1}$, U_0/N, and $\tilde{k}U_0H_0$ as scales of horizontal velocity, horizontal length, time, vertical length, and vertical velocity, and after some algebraic manipulations, Eqs. (2.1)–(2.5) are reduced to

$$\left(\frac{\partial}{\partial t} + iU(t)\right)\left(\frac{\partial}{\partial t} + iU(t)\right)\frac{\partial^2 w_1}{\partial z^2} - w_1 = 0 \tag{2.6}$$

$$w_1(t, z = 0) = iU(t). \tag{2.7}$$

To unravel the nonlinear temporal dependence inherent in (2.6), we follow Bell (1975) and solve (2.6) in a reference frame fixed with respect to the basic flow. This is done by introducing the variable $w(t, z)$ defined as

$$w(t, z) = w_1(t, z)\exp\left(+i\int_0^t U(s)ds\right).$$

Then, Eqs. (2.6) and (2.7) become

$$\frac{\partial^4 w}{\partial z^2 \partial t^2} - w = 0 \tag{2.8}$$

$$w(t, z = 0) = +iU(t)\exp\left(+i\int_0^t U(s)ds\right). \tag{2.9}$$

This last substitution is needed to eliminate the time dependence of the coefficients in Eq. (2.6). Equations (2.8)–(2.9) can be solved using time Fourier transform. In the frame fixed with respect to the flow, w is a sum of monochromatic modes with nondimensional intrinsic frequency, $-\omega$, and vertical wavenumber, m, satisfying the dispersion relation, $m = 1/\omega$. The vertical structure of each mode is given by

$$\exp(+i\epsilon mz),$$

where $\epsilon = +1$ is chosen so that the mode propagates upward. In the frame fixed with respect to the topography, the solution reads:

$$w_1 = i \exp\left(-i \int_0^t U(s)ds\right) \times \int_{-\infty}^{+\infty} F(\omega) \exp\left[+i\left(\omega t + \frac{z}{\omega}\right)\right] d\omega \quad (2.10)$$

where $F(\omega)$ measures the amplitude and the phase of the mode of frequency $-\omega$,

$$F(\omega) = \frac{1}{2\pi} \int_{-\infty}^{+\infty} U(t) \exp(+i\psi(t, \omega))dt, \quad (2.11)$$

and the phase ψ is defined by

$$\psi(t, \omega) = \int_0^t U(s)ds - \omega t.$$

In the following, we assume that the transient mean flow is given by

$$U(t) = \frac{1}{2}\left[1 + \cos\left(\frac{\pi t}{t_f}\right)\right] \quad (2.12)$$

for $|t| < t_f$ and $U(t) = 0$ for $|t| > t_f$.

b. Asymptotic expansion of the wave field

1) APPROXIMATION FOR $F(\omega)$

In the quasi-state case, $U(t)$ is a slowly varying function, (i.e., $t_d = -t_f \ll -1$ and $t_f \gg +1$) and Eq. (2.11) can be estimated by the stationary phase method. This method is used because the phase change, $\psi(t, \omega)$, is rapid compared to the amplitude change, $U(t)$. Then, the main contribution to the integral comes from the neighborhood of the stationary points t_i such that

$$\frac{\partial \psi}{\partial t}(t_i, \omega) = U(t_i) - \omega = 0. \quad (2.13)$$

Figure 1 displays the function $U(t)$ when it is given by (2.12). For $\omega < 0$ or $\omega > 1$, a solution to (2.13) does not exist since $0 \leq U(t) \leq 1$ for all t. When $0 < \omega < 1$ (represented on the figure), Eq. (2.13) admits two roots, $t_1(\omega)$ and $t_2(\omega)$. The first stationary point is reached during the ascending period of the incident flow: $t_1(\omega) < 0$. The second one is reached during the descending period of the incident flow: $t_2(\omega) > 0$. Then, the functions $U(t)$ and $\psi(t, \omega)$ are expanded in Taylor series in the neighborhood of $t_1(\omega)$ and $t_2(\omega)$:

$$\psi(t, \omega) = \psi(t_i, \omega) + \frac{(t - t_i)^2}{2} \ddot{\psi}(t_i, \omega) + \cdots \frac{U(t)}{2\pi}$$

$$= \frac{U(t_i)}{2\pi} + \cdots = \frac{\omega}{2\pi} + \cdots$$

for $i = 1, 2$ and provided that $\ddot{\psi}(t_i, \omega) \neq 0$. Then, the integral representation of $F(\omega)$ is estimated by rotating

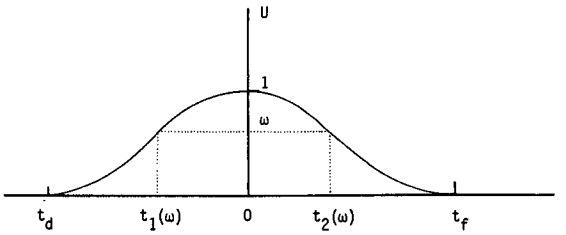

FIG. 1. Normalized incident wind as a function of time. For a given $0 < \omega < 1$, the two moments, t_1 and t_2, are solutions of Eq. (2.13).

the path of integration to the value $\text{sgn}(\dot{U}(t_i))\pi/4$, which corresponds to the path of steepest descent (Lightill 1978). Then, we have

$$F(\omega) \approx \frac{\omega}{2\pi} \sum_{i=1,2} \int_{-\infty}^{+\infty} \exp\left[+i\psi(t_i, \omega) - |\dot{U}(t_i)| \frac{s^2}{2} + i\,\text{sgn}(\dot{U}(t_i))\frac{\pi}{4}\right] ds$$

$$\approx \frac{\omega}{2\pi} \sum_{i=1,2} \left|\frac{2\pi}{\dot{U}(t_i)}\right|^{+1/2} \times \exp\left(+i\psi(t_i, \omega) + i\,\text{sgn}(\dot{U}(t_i))\frac{\pi}{4}\right). \quad (2.14)$$

It is verified that $F(\omega) \to 0$ when $\omega \to 0$. When $\omega \to 1^-$, the two terms in the expression (2.14) become infinitely large since $\dot{U}(t_1)$ and $\dot{U}(t_2)$ tend to 0 (i.e., t_1 and t_2 tend to 0). In this case, the preceding asymptotic development is not valid since both $\ddot{\psi}(t_1, \omega)$ and $\ddot{\psi}(t_2, \omega)$ are 0 when $\omega = 1$. This situation is solved by retaining up to third powers of t in the expansion:

$$\psi(t, \omega) = (1 - \omega)t + \ddot{U}(0)\frac{t^3}{6} + \cdots$$

and retaining only the first term in the Taylor series of $U(t)$:

$$U(t) = 1 + \cdots.$$

By changing the path of integration to the one of steepest descent, the solution is (Lightill 1978, 385–399):

$$F(\omega) \approx \frac{1}{2\pi} \int_{\infty\exp[-(\pi i/6)]}^{\infty\exp[-(5\pi i/6)]} \times \exp\left(+i(1 - \omega)t + i\ddot{U}(0)\frac{t^3}{6}\right) dt,$$

which can be expressed in terms of Airy functions, introducing

$$Sx = (\omega - 1)t \quad \text{and} \quad S^3 = -\frac{\ddot{U}(0)}{2} t^3$$

$$\text{Ai}(x) \approx \frac{1}{2\pi} \int_{\infty\exp(5\pi i/6)}^{\infty\exp(\pi i6)} \exp\left(iSx + i\frac{S^3}{3}\right) dS.$$

Thus, the asymptotic form of $F(\omega)$ is

$$F(\omega) = \left(-\frac{\ddot{U}(0)}{2}\right)^{-1/3} \mathrm{Ai}\left[\left(-\frac{\ddot{U}(0)}{2}\right)^{-1/3}(\omega - 1)\right]. \tag{2.15}$$

Due to the properties of the Airy function, $F(\omega)$ decays exponentially for $\omega > 1$ and becomes oscillatory for $\omega < 1$. This allows a quick and smooth transition to be made between the oscillatory solution (2.14), which is valid for $\omega < 1$ and the solution $F(\omega) = 0$ which is valid for $\omega > 1$. Figure 2 displays the function $F(\omega)$ determined from the equations (2.14) and (2.15) when $U(t)$ satisfies (2.12) and $t_f = 207$. Figure 2 shows how properly the approximations (2.14) and (2.15) match near $\omega = 1$.

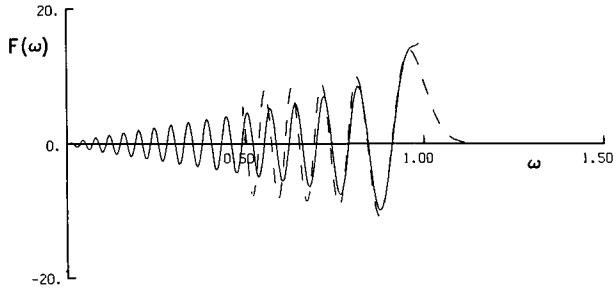

FIG. 2. $F(\omega)$ when $U(t)$ is given by (2.12) and $t_f = 207$: (solid) $F(\omega)$ as given by (2.14); (dashed) $F(\omega)$ as given by (2.15).

2) APPROXIMATION OF THE WAVE FIELD

The next step in the approximation of the exact solution (2.10) consists in applying steepest descent methods in the ω integration, using the preceding approximate form of $F(\omega)$. Considering the asymptotic behavior of the solution (2.10) for large z and t values (i.e., $z \gg 1$ and $t \ll 1$). Note that in dimensional form, the assumption of large z (or t) consists in estimating the wave field at a distance (or a time) that is large (or long) compared to one characteristic vertical wavelength (or period) of the waves. Note also that when a slowly varying wind ceases, $t > t_f \gg 1$, the assumption of large t follows the assumption of slowly varying wind. Then, we can consistently introduce the preceding asymptotic form of $F(\omega)$ into (2.10). Furthermore, we assume that on each side of the ray $z = t$ (which corresponds to the ray of intrinsic frequency, $-\omega = -1$), the wave solution can be approximated with $F(\omega)$ given by Eq. (2.14). Then, (2.10) becomes,

$$w_1(t, z) \approx +i \exp\left(-i \int_0^t U(s)ds\right) \times \sum_{i=1,2} \int_{-\infty}^{+\infty} \omega |2\pi \dot{U}(t_i)|^{-1/2} \times \exp\left[+i\left(\phi_i(\omega, t, z) + \mathrm{sgn}(\dot{U}(t_i))\frac{\pi}{4}\right)\right] d\omega \tag{2.16}$$

where the phase ϕ_i is

$$\phi_i(\omega, t, z) = \int_0^{t_i(\omega)} U(s)ds - \omega t_i(\omega) + \omega t + \frac{z}{\omega}.$$

For the time being, z and t are fixed parameters, and only the dependence on ω is displayed in ϕ_i. Then, for large z and t, the main contribution to the integrals in (2.16) is from the neighborhood of the stationary points ω_s such that

$$\frac{\partial \phi_i}{\partial \omega}(\omega_s, t, z) = \phi_i'(\omega_s, t, z) = t - t_i(\omega_s) - \frac{z}{\omega_s^2} = 0 \tag{2.17}$$

$i = 1, 2$. These are the equations of two rays that describe the propagation of wave packets whose vertical group velocities are ω_s^2. Each wave packet was generated at the ground at the time $t_i(\omega_s)$. Thus, to calculate the amplitude of the wave at a given (z, t), it is necessary to determine the intrinsic frequency, ω_s, of the wave packets reaching (z, t). Figure 3 displays the location of these rays in the (z, t) plane. To represent the rays, we consider that at each initial time t_I, a wave packet is generated at the ground. Its intrinsic frequency is $-\omega_I = -U(t_I)$. Its vertical wavenumber is $m_I = 1/\omega_I$. For $t > t_I$, this wave packet propagates along the ray:

$$z = \omega_I^2(t - t_I).$$

In Fig. 3, 13 rays are represented for 13 values of t_I, $t_d < t_I < t_f$, and $U(t)$ is given by (2.12). It shows that the (z, t) plane is separated into three regions. In region I, no wave arrives and Eq. (2.17) does not give a saddle point. In region II, the solution is the superposition of waves, generated during the ascending period of the mean flow. In this area, Eq. (2.17) gives two saddle points ω_s ($s = 1, 2$). They correspond to waves generated at times $t_1(\omega_1) < 0$ and $t_1(\omega_2) < 0$ [both saddle points contribute to the first integral in (2.16)]. Region I and region II are separated by the caustic defined as the intersection of all the rays of the wave packets generated during the ascending period of the mean flow. It is the wave front of the solution: at a given t it is the maximum height reached by the wave packets. In region III ($z < t$) the solution is the superposition of waves generated when the wind increases, and of waves generated when it decreases: at any point in this region Eq. (2.17) gives two saddle points ω_s ($s = 1, 2$) corresponding to wave packets generated at the times $t_1(\omega_1) < 0$ and $t_2(\omega_2) > 0$. Then, the first and the second saddle points contribute to the first and the second integral in (2.16), respectively. At the boundary be-

tween regions (II) and (III) (around the ray $z = t$), there are rays corresponding to wave packets for which ω is close to 1. There, $F(\omega)$ has to be considered as given by (2.15) instead of (2.14). We will see that such a matching between regions II and III is not necessary.

The preceding ray equations are consistent with the usual ray tracing theory. At $t = t_I$ a stationary wave is generated at the ground: its relative frequency is $\omega_r = -\omega = -U(t_1)$. Its vertical wavenumber, m, is given by the dispersion relation, $m = \omega^{-1}$. Thereafter, since the medium does not change in z, the vertical wavenumber, m, of the wave is conserved (Lightill 1978). As it is related to the intrinsic frequency through the dispersion relation, the latter is also conserved and the wave propagates along a straight ray in the (z, t) plane.

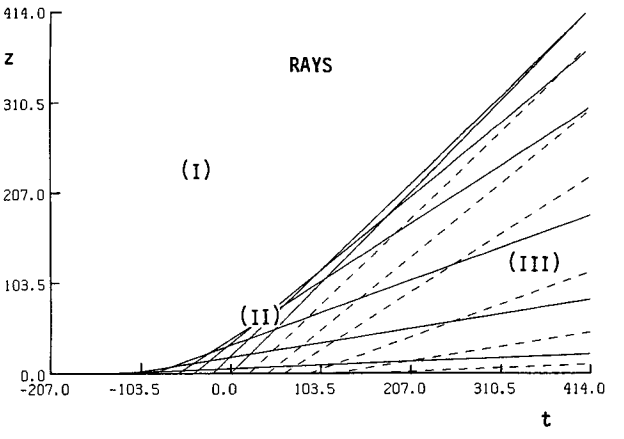

FIG. 3. Rays of wave packet propagation in the (z, t) plane: (solid) wave packets generated during the ascending period of the incident wind; (dashed) wave packets generated during the decreasing period of the incident wind. Same conditions as Fig. 2.

(i) *Approximation of the solution in the wave regions (I) and (II): $z > t$*

Above the ray $z = t$, only waves generated during the ascending period of the mean flow are present, since no saddle points corresponding to waves generated during the decreasing period of the mean flow can be found in this area of the (z, t) plane. Consequently, no saddle points corresponding to $i = 2$ occur, and the equation (2.16) is approximated by:

$$w_1(z, t) \approx i \exp\left(-i \int_0^t U(s)ds\right) \times \int_{-\infty}^{+\infty} \omega(2\pi \dot{U}(t_1(\omega)))^{-1/2} \times \exp\left[+i\left(\phi_1(\omega, t, z) + \frac{\pi}{4}\right)\right]. \quad (2.18)$$

As seen in Fig. 3, for $z > t$, a caustic exists; it is the boundary between regions of complicated wave field and a neighboring region including no wave. Before, this caustic was defined geometrically. Mathematically, in systems analyzed using the method of the stationary phase, the difficulty arises when the second derivative of the phase (with respect to the integration parameter, i.e., ω) vanishes. Thus, the ray equation:

$$\phi_1'(\omega_{1c}, t, z) = t - t_{1c} - \frac{z}{\omega_{1c}^2} = 0, \quad \text{where} \quad t_{1c} = t_1(\omega_{1c}) \quad (2.19a)$$

with the condition,

$$\phi_1''(\omega_{1c}, t, z) = -t_{1c}' + \frac{2z}{\omega_{1c}^3} = 0, \quad \text{where} \quad t_{1c}' = t_1'(\omega_{1c}), \quad (2.19b)$$

forms the parametric equations (with parameter ω_{1c}) of the caustic [i.e., the envelope of the rays (2.17, $i = 1$) in the (z, t) plane]. This caustic is represented in Fig. 4. In the neighborhood of the caustic, the solution is estimated by developing the phase and the amplitude in equation (2.18) as

$$\phi_1(\omega, t, z) = \psi(t_{1c}, \omega_{1c}) + \omega_{1c}t + \frac{z}{\omega_{1c}} + \left((t - t_{1c}) - \frac{z}{\omega_{1c}^2}\right)(\omega - \omega_{1c}) - \left(t_{1c}'' + \frac{6z}{\omega_{1c}^4}\right)\frac{(\omega - \omega_{1c})^3}{6} + \cdots$$

amplitude

$$= +i \exp\left(-i \int_0^t U(s)ds\right)\omega_{1c}(2\pi \dot{U}(t_{1c}))^{-1/2} + \cdots.$$

Then, the parameter ω_{1c} is defined as a function of z by the equation (2.19b), and the integral (2.18) is estimated by changing the path of integration to that of the steepest descent. Since it has been verified that

$$\phi_1'''(\omega_{1c}, t, z) = \left(t_{1c}'' + \frac{6z}{\omega_{1c}^4}\right) > 0,$$

the solution (2.18) is approximated by

$$w_1 \approx i \exp\left(-i \int_0^t U(s)ds\right)\omega_{1c}(2\pi \dot{U}(t_{1c}))^{-1/2} \exp\left[+i\left(\psi(t_{1c}, \omega_{1c}) + \omega_{1c}t + \frac{z}{\omega_{1c}} + \frac{\pi}{4}\right)\right] \times \int_{\infty \exp[-(\pi i/6)]}^{\infty \exp[-(5\pi i/6)]} \exp\left[i(t - t_{1c}) - \frac{z}{\omega_{1c}^2}\right)s - \left(t_{1c}'' + \frac{6z}{\omega_{1c}^4}\right)\frac{s^3}{6}\Bigg]ds,$$

which can be expressed in terms of the Airy function $\mathrm{Ai}(x)$ by introducing suitable variables:

$$xS = \frac{z}{\omega_{1c}^2} - (t - t_{1c})s; \quad S^3 = \left(\frac{t''_{1c}}{2} + \frac{3z}{\omega_{1c}^4}\right).$$

The asymptotic expression of w_1 in the vicinity of the wave front becomes

$$w_1 \approx +i \exp\left(-i \int_0^t U(s)ds\right)\omega_{1c}(2\pi\dot{U}(t_{1c}))^{-1/2} \times \exp\left[+i\left(\psi(t_{1c}, \omega_{1c}) + \omega_{1c}t + \frac{z}{\omega_{1c}} + \frac{\pi}{4}\right)\right]\frac{2\pi}{S}\,\mathrm{Ai}\left(\frac{z/\omega_{1c}^2 - (t - t_{1c})}{S}\right). \quad (2.20)$$

Due to the properties of the Airy function, the amplitude of the solution decreases toward 0 above the caustic. Below the caustic, it varies like a cosine function.

(ii) *Approximation of the solution in the wave region (III):$z < t$*

Below the ray $z = t$, the waves are generated during both ascending and descending periods of the mean flow. Then, the phase and the amplitude in the integrals of (2.16) are expanded around the stationary points ω_i ($i = 1, 2$):

$$\phi_i(\omega, t, z) \approx \psi(t_i, \omega_i) + \omega_i t + \frac{z}{\omega_i} + \frac{(\omega - \omega_i)^2}{2}\phi''(\omega_i, t, z)$$

$$\text{amplitude} = i \exp\left(-i \int_0^t U(s)ds\right)\omega_i |2\pi\dot{U}(t_i)|^{-1/2}.$$

Furthermore, for both saddle points it is found that

$$\phi''(\omega_i, t, z) = \frac{2z}{\omega_i^3} - t'_i > 0.$$

Then, the two integrals in Eq. (2.16) are reduced to the real error integral by changing the paths of integration through $+\pi/4$:

$$w_1 \approx i \exp\left(-i \int_0^t U(s)ds\right) \times \sum_{i=1,2} \omega_i |\dot{U}(t_i)|^{-1/2}(2z/\omega_i^3 - t'_i)^{-1/2} \times \exp\left[+i\left(\psi(t_i, \omega_i) + \omega_i t + \frac{z}{\omega_i} + (2 - i)\frac{\pi}{2}\right)\right]. \quad (2.21)$$

(iii) *Discussion*

In Fig. 4, the profiles of the wave amplitude and phase velocities are shown after the wind stops ($t = t_f$, $2t_f$, $3t_f$); $U(t)$ is given by (2.12) and $t_f = 207$. Below the ray $z = t$, the wave local phase velocities c_1 and c_2 (i.e., $-\omega_1$ and $-\omega_2$) and the wave-induced vertical velocity are calculated using (2.17) and (2.21), respectively. Above this ray, they are calculated using (2.19) and (2.20), respectively. Furthermore, the shape of the solution in the vicinity of $z = t$ is drawn in Fig. 5. It shows how expressions (2.17) and (2.21) match just below the ray $z = t$. The Airy integral interpolates from the calm upper atmosphere (region (I) to the region (III) where the wave amplitude varies as a succession of bulges and nodes. There, the solution results from the beats between waves of close amplitude and wavelength. This can be seen as the interference between a first system of gravity waves generated while the incident wind increases and a second system of gravity waves generated while it decreases. Figure 4 also shows that the wave amplitude is at its maximum just below the wave front. This is normal since the waves there have been generated at the ground when the wind was nearly at its maximum.

The highly dispersive character of the wave should also be noted. As shown in Fig. 4, it is found that the maximum amplitude of the wave field decreases in time. It is also found that the extension of each bulge grows in time, allowing for the wave field to take up the whole space between the ground and the caustic. This spreading is a consequence of the broad spectrum of waves forced at the ground during the gust of wind: the function $F(\omega)$ is different from zero in the whole interval $0 < \omega \leqslant 1$.

Figure 4 also shows the vertical profiles of the absolute phase velocities, $c = U(t) - \omega$. After the wind stops, $U(t) = 0$, and ω varies from 0 to +1 as z varies from the ground to the caustic. Consequently, c varies between 0 and −1 in the same way. The waves present near the caustic are the most unsteady since they were generated at the ground when the incident wind amplitude was maximum [$\omega \approx U(0) = 1$ and $c \approx -1$]. This shows that most of the waves forced on the mountain are very unsteady after the wind stops.

This behavior characterizes the quasi-steady regime. In this context, we further found that the number of bulges decreases when the duration of the wind decreases: when t_f approaches 0, the number of bulges approaches 1.

3) Spatial Propagation of Nonstationary Topographic Waves

For a nonmonochromatic mountain, the linear wave solution is the sum of zonal harmonics, each particular harmonic being generated at the location of the mountain. Then, the spatial propagation of the different waves generated during the wind is determined by cal-

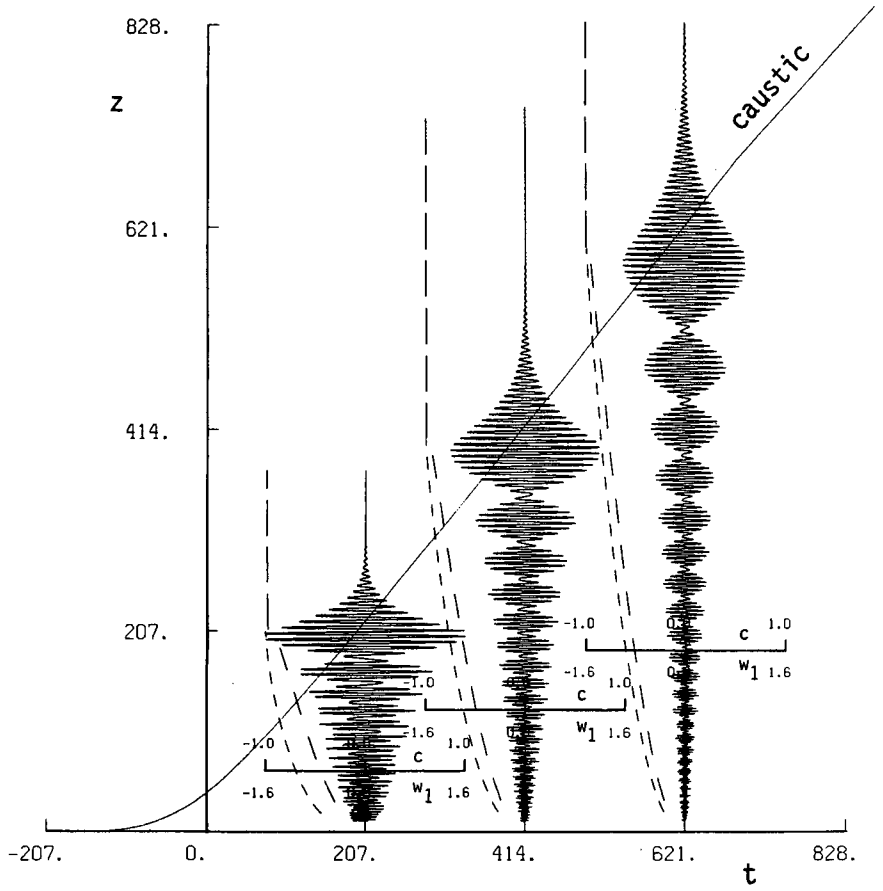

FIG. 4. Wave field at three different times: (solid) vertical velocity $w_1(z)$; (long dashed) phase velocity above the caustic, c_{1c}; (medium dashed) phase velocity below the caustic for waves generated during the ascending period of the incident wind, c_1; (short dashed) phase velocity below the caustic for waves generated during the decreasing period of the incident wind, c_2. Same conditions as Fig. 2.

culating the rays of propagation of the packets in the (x, z) plane:

$$\frac{dx}{dt} = C_{gx} + U(t), \quad \text{where} \quad C_{gx} = \frac{\partial \omega_r}{\partial k} = \omega_r = \text{cte}$$

$$\frac{dz}{dt} = C_{gz}, \quad \text{where} \quad C_{gz} = \frac{\partial \omega_r}{\partial m} = \omega_r^2 = \text{cte}.$$

Each value of $\omega_r \in]-1, 0[$, corresponds to two wave packets, generated at $t_1(-\omega_r)$ and $t_2(-\omega_r)$. Their trajectories in the (x, z) plane are given by the parametric equations (with parameter t):

$$\left.\begin{aligned} x &= \omega_r(t - t_i(-\omega_r)) + \int_{t_i(-\omega_r)}^{t} U(s)ds \\ z &= \omega_r^2(t - t_i(-\omega_r)) \end{aligned}\right\},$$

$$\text{for} \quad t > t_i(-\omega_r) \quad \text{and} \quad i = 1, 2.$$

Nine of those rays are represented in Fig. 6. They correspond to the relative frequencies $\omega_r = -0.2, -0.4, -0.6, -0.8, -1$. The locations reached by each packet at various moments (t_f, $2t_f$, $3t_f$, ...) are also represented by numbers (1, 2, 3, ..., respectively). Figure 6 shows that the wave packets generated during the growing phase of the wind first propagate leeward of the mountain. In fact, a wave packet is stationary when it is generated at the ground and its horizontal group velocity is opposite to the incident wind. When the latter increases, the group velocity is no longer balanced and the packet propagates downstream. The direction of propagation reverses during the decreasing phase of the flow, when the incident wind becomes smaller than the opposite of the horizontal group velocity of the packet. The wave packets generated during the decreasing phase of the wind always propagate windward because the incident wind is always smaller than the one existing when they were generated. Nevertheless, note that during the wind all the waves remain close to the mountain. After the wind stops, all the waves propagate windward. Figure 6 also shows that the largest waves (those with relative frequency close to -1) propagate fastest windward the mountain.

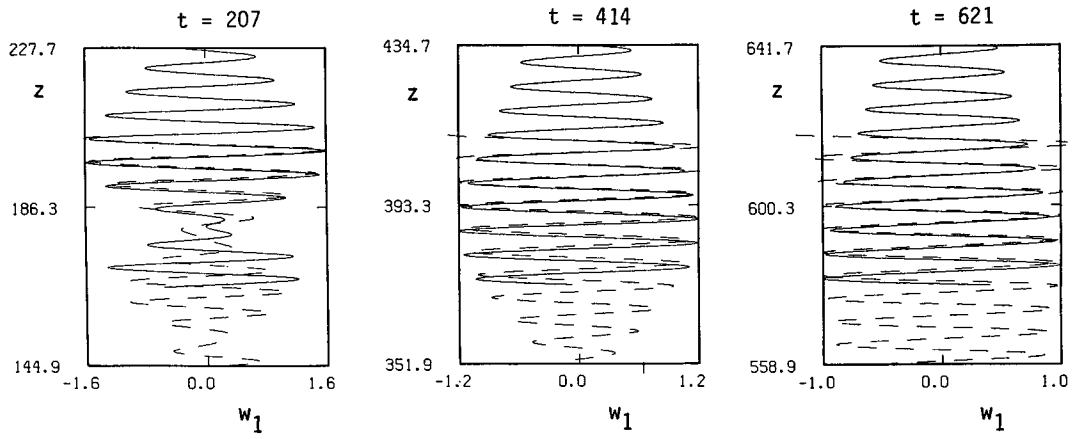

FIG. 5. Enlargement of the solution: (solid) $w_1(z)$ is calculated using (2.20); (dashed) $w_1(z)$ is calculated using (2.21). Same conditions as Fig. 2.

3. Numerical simulations

a. The model

In this section, the dynamics of topographic waves generated by a transient wind is investigated using a two-dimensional $(\tilde{x}, \tilde{z})$, linear time-dependent model in Boussinesq approximation. The incident flow, which varies in time and in vertical direction, is written as

$$\tilde{u}_0(\tilde{t}, \tilde{z}) = U_0 u_v(\tilde{t}) u_c(\tilde{z})$$

and $U_0 = 10\ \text{m s}^{-1}$. The streamfunction, $\tilde{\Psi}_1$, the buoyancy force, $\tilde{b}_1$, and the vorticity, $\tilde{\zeta}_1$, associated with the topographically induced disturbance are defined by

$$\tilde{u}_1 = \frac{\partial \tilde{\Psi}_1}{\partial \tilde{z}}; \quad \tilde{w}_1 = -\frac{\partial \tilde{\Psi}_1}{\partial \tilde{x}}; \quad \tilde{b}_1 = -g\left(\frac{\tilde{\rho} - \tilde{\rho}_0}{\tilde{\rho}_0}\right)_1$$

$$\tilde{\zeta}_1 = \frac{\partial \tilde{u}_1}{\partial \tilde{z}} - \frac{\partial \tilde{w}_1}{\partial \tilde{x}} = \left(\frac{\partial^2 \tilde{\Psi}_1}{\partial \tilde{z}^2} + \frac{\partial^2 \tilde{\Psi}_1}{\partial \tilde{x}^2}\right). \quad (3.1)$$

The equations of motion are written in the streamfunction vorticity form:

$$\left(\frac{\partial}{\partial \tilde{t}} + \tilde{u}_0 \frac{\partial}{\partial \tilde{x}}\right)\tilde{\zeta}_1 - \frac{d^2 \tilde{u}_0}{d\tilde{z}^2}\frac{\partial \tilde{\Psi}_1}{\partial \tilde{x}} + \frac{\partial \tilde{b}_1}{\partial \tilde{x}} + \tilde{a}\tilde{\zeta}_1 + \frac{d\tilde{a}}{d\tilde{z}}\frac{\partial \tilde{\Psi}_1}{\partial \tilde{z}} - \nu \Delta \zeta_1 = 0 \quad (3.2)$$

$$\left(\frac{\partial}{\partial \tilde{t}} + \tilde{u}_0 \frac{\partial}{\partial \tilde{x}}\right)b_1 - N^2 \frac{\partial \tilde{\Psi}_1}{\partial \tilde{x}} + \tilde{a}\tilde{b}_1 - \nu \Delta \tilde{b}_1 = 0; \quad (3.3)$$

they are valid whatever the time scale of the incident wind variations. Furthermore, Δ is the Laplacian operator, $\tilde{\rho}_0(\tilde{z})$ is the basic-state density profile, $N^2 = 4 \times 10^{-4}\ \text{s}^{-2}$ is the buoyancy frequency, $\tilde{a}$ is a linear damping coefficient, and ν is the molecular diffusion. The boundaries of this model require special consideration. At the bottom, the topographic gravity waves are forced through the condition:

$$\tilde{\Psi}_1 = -\tilde{u}_0 \tilde{h} \quad \text{at} \quad \tilde{z} = 0. \quad (3.4)$$

In order to prevent undesirable wave reflection at the upper boundary, a 30-km sponge layer is used. In this layer, the damping coefficient $\tilde{a}$ increases smoothly from zero to 2, 5 $\tilde{k} U_0$. The domain extension is 190 km in the vertical direction, and the upper boundary condition is

$$\tilde{\Psi}_1 = 0 \quad \text{at} \quad \tilde{z}_T = 190\ \text{km}.$$

This ensures that no mean transport occurs in addition to the one specified through $\tilde{u}_0$. In the horizontal direction, periodic boundary conditions are applied. The

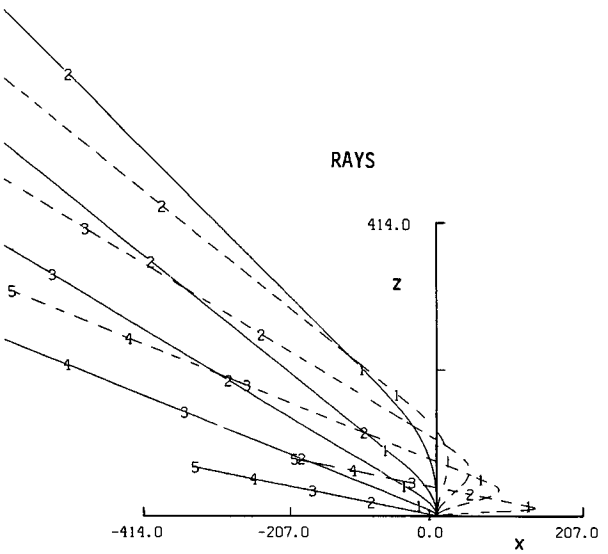

FIG. 6. Rays of wave propagation in the (x, z) plane: (dashed) waves generated during the ascending period of the mean flow; (solid) waves generated during the decreasing period of the mean flow. Same conditions as Fig. 2.

spatial derivatives in the x and z directions are calculated with centered finite differences. Thirty-two points are used in the horizontal direction. It is found that this is accurate enough to represent the vertical propagation of the single horizontal harmonic wave considered in this study. The total horizontal length of the field corresponds to one wavelength, $2\pi/\tilde{k}$, of the corrugated bottom:

$$\tilde{h}(\tilde{x}) = H_0 \cos(\tilde{k}\tilde{x}).$$

Note that the use of a two-dimensional model to study the monochromatic wave field resulting from this ground forcing is not necessary: a simpler (one dimensional) model with Fourier representation of the wave field would give similar results. Nevertheless, as we disposed of a performant two-dimensional model, we used it in the present study. In experiments for which the mean flow is uniform in the vertical direction, the grid is uniform and 512 points are used in the vertical direction. When the mean flow varies in the vertical direction, a stretched grid with 1024 points is introduced to allow for a small vertical grid spacing in the shear layer. Indeed, since the waves can reach critical levels in the shear layer, a particularly fine vertical resolution is required there. In this case, we also introduce a small viscosity, $\nu \neq 0$, and the step length used is always smaller than the viscous scale,

$$l_\nu = \left(\frac{\tilde{k}}{\nu}\frac{d\tilde{u}_0(\tilde{z})}{d\tilde{z}}\right)^{-1/3},$$

introduced by Hazel (1967). For a wave of absolute phase velocity $\tilde{c}$, reaching a critical level at $\tilde{z}$ [i.e., $\tilde{u}_0(\tilde{z}) = c$], l_ν characterizes the depth of the layer surrounding $\tilde{z}$ where the diffusion is important. Our numerical experiments revealed that this vertical resolution was sufficient for convergence of the solution. The temporal integration of (3.2) and (3.3) are performed with the predictor corrector algorithm used by Lindzen and Barker (1985). The vertical integration of the streamfunction equation (3.1) is done with a Gaussian elimination technique.

b. *Validation of the analytic results*

In this subsection, we verify the validity of the analytical calculations presented in section 2. The incident wind is given by

$$u_v(\tilde{t}) = \frac{1}{2}\left[1 + \cos\left(\pi\frac{\tilde{t} - \tilde{t}_f}{\tilde{t}_f}\right)\right]$$

$$\text{for} \quad 0 \leq \tilde{t} \leq \widetilde{2t_f}; \quad u_v(\tilde{t}) = 0,$$

$$\text{elsewhere;} \quad u_c(\tilde{z}) = 1. \quad (3.5)$$

The maximum mountain height is $H_0 = 100$ m so the inverse Froude number is 0.2, ensuring that the linear approximation is justified. The mountain's horizontal wavelength is $\tilde{\lambda} = 2\pi/\tilde{k} = 13.1$ km. With the parameters given above, the nondimensional time, $t_f = 207$, corresponds to $\tilde{t} = 12$ h in dimensional units. Figure 7a represents the vertical profiles of the vertical velocity, $\tilde{w}_1$, and that of the wave horizontal phase velocity, $\tilde{c}_1$, obtained through numerical calculations at the wind stops ($\tilde{t} = 2\tilde{t}_f = 1$ day). In order to make the comparison with theoretical results easier, all the parameters are represented in dimensional as well as in nondimensional form. Figure 7b represents the theoretical solution obtained in section 2. Comparison of Fig. 7a and Fig. 7b shows that the characteristics of the wave amplitude vertical variation, analyzed theoretically in section 2, are also obtained with the numerical model. In the numerical model, the phase velocity of the solution is determined by analyzing the change in the phase of the solution between $\tilde{t}$ and $\tilde{t} + d\tilde{t}$, at a given horizontal location. This procedure is not valid at grid points where the amplitude of the wave falls to zero. Furthermore, this numerical evaluation of the phase velocity does not allow separation of the solution between the two different groups of waves interfering below the caustic. Note that their presence is proved by the beat in amplitude observed in the vertical direction. In this case it is found that the "numerical" phase velocity is close to $-U_0$ above the caustic and increases to 0 as $\tilde{z}$ decreases to 0. In all the cases, it is found to be close to the analytical values.

c. *Extension to rapid wind*

It has been found, by performing different comparisons of this kind, that the quality of the analytical approximation weakens when $\tilde{t}_f$ decreases (the other parameters remain unchanged). This is not surprising since the asymptotic developments performed in section 2 are based on the quasi-steady assumption. Then the generation of topographic waves when the wind varies rapidly has to be studied numerically. In the preceding configuration, the transient wind is rapid when it lasts 2 h. Such is the case in Fig. 8, where the wind time dependence is given by (3.5) and $\tilde{t}_f = 1$ h. When the wind stops ($\tilde{t} = 2\tilde{t}_f = 2$ h; Fig. 8a), the wave field presents one main bulge. A node for the solution occurs near the ground. The arrows in the Fig. 8 represent the location of the caustic [as given by (2.19)]. The maximum amplitude of the wave is just below the caustic: it is close to the ground. Besides, the phase velocity of the wave is consistently negative and varies between 0 (at the ground) and $-2U_0$ (far above the caustic). At the caustic, it is $-U_0$. Thereafter ($\tilde{t} = 6$ h in Fig. 8b and $\tilde{t} = 12$ h in Fig. 8c), it appears that the wave field presents two bulges separated by one node. With increasing time, the vertical extension of the bulges increases due to wave dispersion. Then, the vertical propagation of the wave front and the vertical dispersion of the frontal bulge combine together to

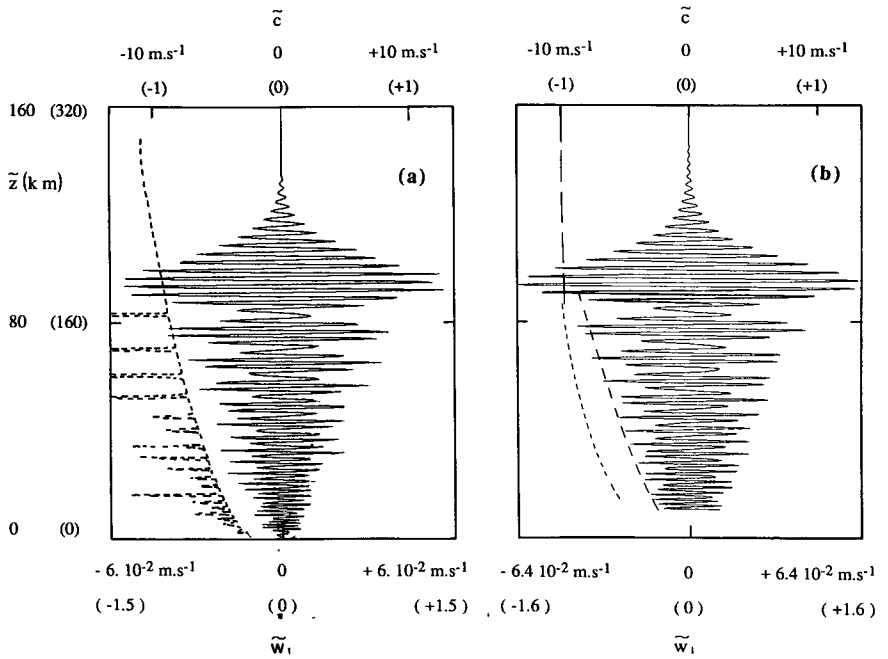

FIG. 7. Comparison between analytical and numerical results. (a) numerical simulation: (solid); $\tilde{w}_1$, (short dash) $\tilde{c}$; (b) theory: (solid) $\tilde{w}_1$, (long dash) $\tilde{c}_{1c}$, (dash) $\tilde{c}_1$; (short dash) $\tilde{c}_2$. All quantities are represented in both nondimensional form and dimensional form. Dimensional parameters: $\tilde{\lambda}_x$ = 13.1 km, H_0 = 100 m, U_0 = 10 m s^{-1}, N = 0.02 s^{-1}, $\tilde{t}_f$ = 12 h.

make the wave present in the whole field 10 h after the wind stops.

d. *Wave-induced mean flow fluctuations*

As noted in the Introduction, the importance of transient effects on the gravity wave–mean flow interaction was first demonstrated by Eliassen and Palm (1960). Transient effects induce vertical variations of the momentum flux,

$$F_w(z, t) = \frac{1}{2}\rho_0 \tilde{w}_1^* \tilde{u}_1,$$

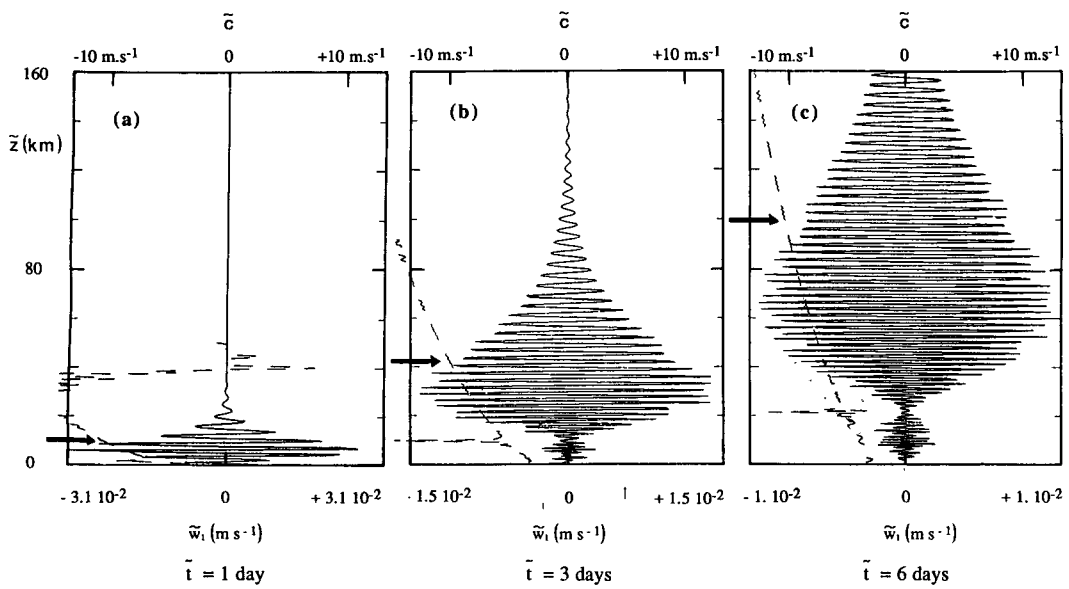

FIG. 8. Vertical wind, $\tilde{w}_1$, at three different times in the case of a rapid gust of wind: arrows represent the theoretical location of the caustic. Dimensional parameters: $\tilde{\lambda}_x$ = 13.5 km, H_0 = 100 m, U_0 = 10 m s^{-1}, N = 0.02 s^{-1}, $\tilde{t}_f$ = 1 h.

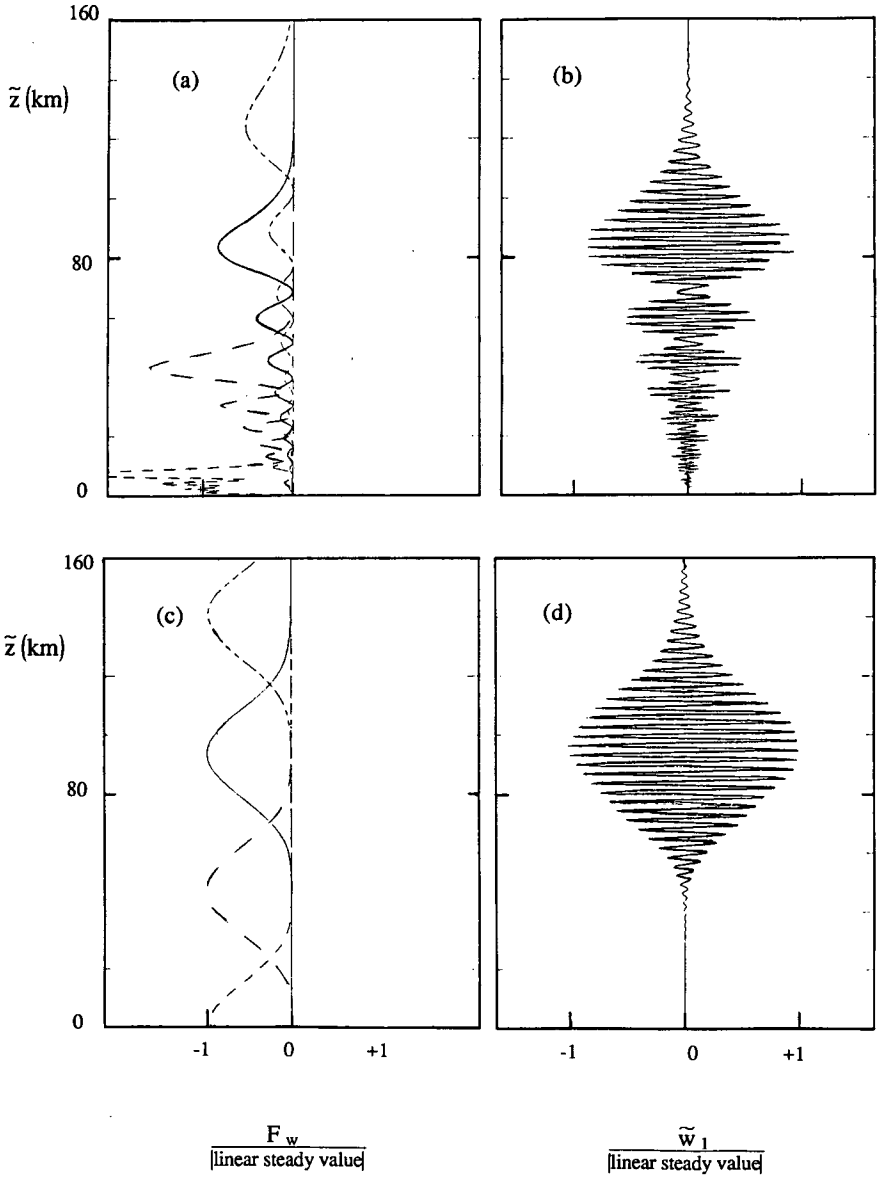

FIG. 9. Comparison of two models of topographic waves. Mountain wave model: (a) momentum flux: (short dash) $\tilde{t} = 6$ h, (medium dash) $\tilde{t} = 12$ h, (solid) $\tilde{t} = 18$ h, (long and short dash) $\tilde{t} = 24$ h; (b) vertical velocity, $\tilde{w}_1$, at $\tilde{t} = 18$ h. Single wave packet model: (c) momentum flux: (short dash) $\tilde{t} = 6$ h, (medium dash) $\tilde{t} = 12$ h, (solid) $\tilde{t} = 18$ h, (medium short medium) $\tilde{t} = 24$ h, (d) $\tilde{w}_{1_2}$ at $\tilde{t} = 18$ h. Dimensional parameters: $\tilde{\lambda}_x = 13.1$ km, $H_0 = 100$ m, $U_0 = 10$ m s^{-1}, $N = 0.02$ s^{-1}, $t_f = 6$ h.

and alter the mean flow. This vertical momentum flux is represented at different times in Fig. 9 when the incident wind is given by (3.5) and $\tilde{t}_f = 6$ h. All the other parameters are those of the preceding experiments. Accordingly, the corresponding nondimensional time scale is $t_f = 103$. Figure 9b shows the wave amplitude at $\tilde{t} = 18$ h. As described previously, it fluctuates in the vertical direction and more than six bulges are present. As expected, the vertical profile of the momentum flux oscillates together with the wave amplitude (Fig. 9a). Ignoring the nonlinear effects on the disturbance, as the self-acceleration of the wave phase velocity through the wave-induced mean flow change (Fritts and Dunkerton 1984), the induced modification of the mean flow at a given altitude can be described as follows. As the frontal bulge arrives, the mean flow is first decelerated because the momentum flux decreases with height. Once the maximum amplitude in

the frontal bulge passes the altitude considered, the mean flow is accelerated and returns to zero when the first node arrives. Thereafter, the other bulges pass, decelerating and accelerating again the mean flow. Nevertheless, the amplitude of these mean flow fluctuations decreases in time because the maximum wave amplitude attained in each bulge decreases with height. These fluctuations of the mean flow also decrease in time because the wave field disperses and the maximum wave amplitude attained in each bulge decreases in time.

This behavior is quite different from the transient effects induced by a vertically propagating single wave packet (Grimshaw 1975). To study transient gravity waves, Dunkerton and Fritts (1984) used a model where the ground-forcing amplitude varies while the frequency is nearly constant. This kind of forcing creates a single wave packet (Fig. 9d). For the study of unsteady mountain waves, this model is unrealistic since it represents waves forced by a constant wind incident over a time-varying mountain. Figure 9c represents the momentum flux induced by such a wave field when the time fluctuation of the maximum elevation, H_0, is given by (3.5) and $\tilde{t}_f = 6$ h. Figure 9c shows that at various times, the vertical profile of the momentum flux remains unchanged and propagates vertically with a well-defined group velocity:

$$\tilde{C}_{gz} \approx 2 \text{ m s}^{-1} \approx \frac{\tilde{k}U_0^2}{N}.$$

This simply illustrates the usual concept of wave packets (Landau and Lifshitz 1959) where the wave amplitude changes in the vertical direction (defining the form of the packet) while the frequency and the wavenumbers change a little so that the wave field does not disperse rapidly. As it propagates vertically this wave packet first decelerates and then accelerates the mean flow, which returns to zero. Furthermore, the maximum amplitude of the momentum flux does not change in time. This is different from the transient mean flow oscillations accompanying topographic wave propagation.

To see if these oscillations are also present when the transient wind is asymmetric, Fig. 10 shows the vertical structure of the Reynolds stress for various types of transient winds. In all these cases, the ascending period remains unchanged while the duration of the decreasing period varies:

$$u_v(\tilde{t}) = \frac{1}{2}\left[1 + \cos\left(\pi \frac{\tilde{t} - \tilde{t}_d}{\tilde{t}_d}\right)\right]$$

for $0 \leq \tilde{t} \leq \tilde{t}_d = 6$ hours

$$u_v(\tilde{t}) = \frac{1}{2}\left[1 + \cos\left(\pi \frac{\tilde{t} - \tilde{t}_d}{\tilde{t}_f}\right)\right]$$

for $\tilde{t}_d \leq \tilde{t} \leq \tilde{t}_d + \tilde{t}_f$ (3.6)

$$u_v(\tilde{t}) = 0, \quad \text{elsewhere.}$$

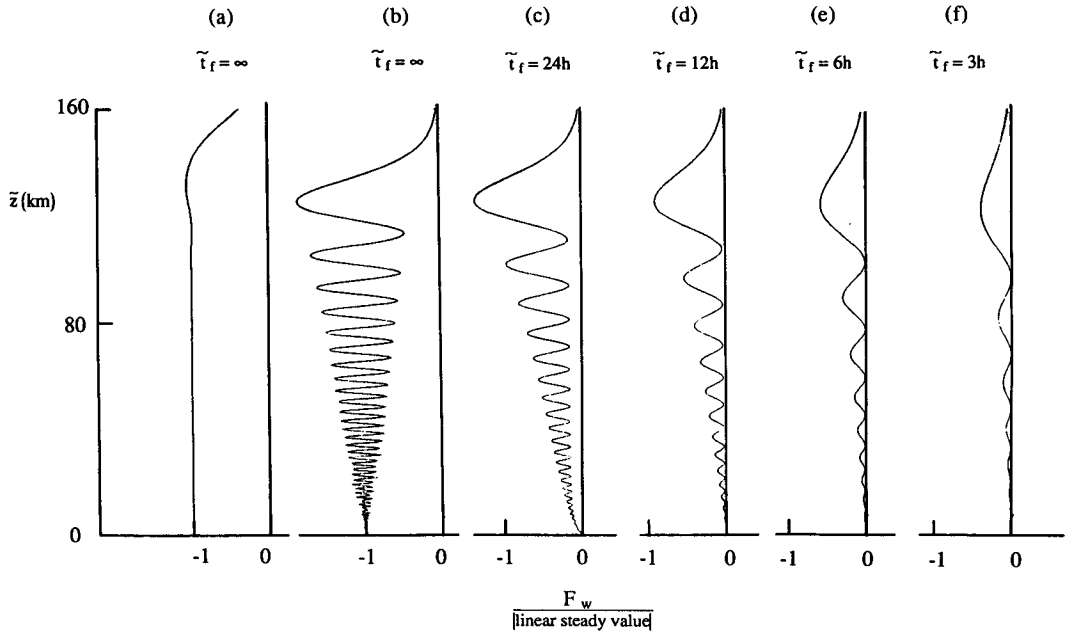

FIG. 10. Momentum flux associated with an asymmetric gust of wind at $\tilde{t} = 24$ h. (a) Single wave packet model; (b), (c), (d), (e), and (f) mountain wave model. Dimensional parameters: $\tilde{\lambda}_x = 13.1$ km, $H_0 = 100$ m, $U_0 = 10$ m s^{-1}, $N = 0.02$ s^{-1}, $\tilde{t}_d = -6$ h.

We further consider the five cases: $\tilde{t}_f = 3, 6, 12, 24, \infty$ h. Figure 10 shows that in all the cases, the Reynolds stress oscillates in the vertical direction. As long as the decreasing time, $\tilde{t}_f \leqslant \tilde{t}_d$ (Figs. 10e and 10f), it is a succession of bulges and nodes, the wave amplitude being zero at the nodes. For larger decreasing time (Figs. 10b, 10c, 10d), this oscillatory structure is still observed but the wave amplitude no longer falls to zero at the nodes. Furthermore, the number of bulges present increases when the decreasing time, $\tilde{t}_f$, increases. At the limit, $\tilde{t}_f = \infty$ (Fig. 10b), the oscillations of the momentum flux are also very large: they are of the order of magnitude of the linear stationary momentum flux. In this case, the transient effects observed when topographic waves are forced by a growing wind remains very large once the wave front has passed. These transient effects do not occur when the waves are forced by a growing mountain (Fig. 10a). This last result is important since this procedure is sometimes used to force gravity waves in models of transient wave–mean flow interaction (Dunkerton 1981).

e. *Unsteady topographic waves forced by a vertically varying wind*

In the troposphere, the rapid changes of the wind intensity are often associated with the passage of a front. An example of the interaction between a synoptic front and topography is reported by Smith (1984), in the context of lee cyclogenesis. This author has shown that an important characteristic of the incident wind is that it can reverse in the vertical direction. Moreover, the interaction of topographic gravity waves with a zero-level wind, $\tilde{z}_0$, is known to have important consequences on the atmospheric dynamics in the vicinity of mountains (Clark and Peltier 1984). When the incident flow is stationary, these authors have shown that mountain waves encounter a critical level at $\tilde{z}_0$, because they are steady. The waves are nonlinearly reflected at the shear layer and they are trapped between the ground level and $\tilde{z}_0$. In some cases, resonance occurs that leads to downslope windstorms. An indirect result of this work is that the wave remains poorly transmitted through the shear layer (see Fig. 7 in their work). As in the linear case (Booker and Bretherton 1967; Eliassen and Palm 1960), steady topographic waves do not go through a level of zero wind. When the wind varies in time, the ground-generated waves can be unsteady as they reach the shear layer. The waves do not necessarily encounter critical levels and can propagate freely toward the middle atmosphere although the incident wind is always zero at $\tilde{z}_0$.

In the following experiments, the vertical variation of the mean flow is given by

$$\tilde{u}_c(\tilde{z}) = \tanh\left(\frac{\tilde{z}_0 - \tilde{z}}{D}\right). \qquad (3.7)$$

Here D and $\tilde{z}_0$ are the depth and the altitude of the shear layer, respectively. The temporal evolution of the mean flow is given by (3.5), $\tilde{t}_f = 6$ h, and we consider the experiments: $D = 1000$ m and $\tilde{z}_0 = 12.5$ km, 25 km, 50 km. The distance $\tilde{z}_0$ is chosen so that the time,

$$\tilde{t}_w = \tilde{z}_0/(\tilde{C}_{gz})_{\max} \approx \tilde{z}_0 N/\tilde{k}U_0^2 = 1 \text{ h } 30 \text{ min}, 3 \text{ h}, 6 \text{ h},$$

required for the largest amplitude wave packets to reach the shear layer, is less than or equal to the unsteady time scale, $\tilde{t}_f$. In the linear approximation, the waves that encounter a critical level are absorbed because the minimum Richardson number,

$$\mathrm{Ri} = \frac{N^2}{(\tilde{u}_0)_{,\tilde{z}}^2} \geqslant \frac{N^2 D^2}{U_0^2} = 4,$$

is always large (Booker and Bretherton 1967). This result remains valid in the viscous case at large Reynolds number (Hazel 1967). However, the use of the linear approximation to study critical-level interaction requires caution. In fact, the nature of the critical-level regime depends on the relative sizes of the viscous scale, l_ν, and of the nonlinear scale, l_n,

$$l_n \approx \epsilon^{2/3} D,$$

defined by Brown and Stewartson (1980). Here ϵ is the normalized amplitude of the incident wave: $\epsilon = H_0/D$. It characterizes the depth of the layer, surrounding a critical level where the nonlinearities are important. In the following experiments, $H_0 = 10$ m and $\nu = 1$ m^2 s^{-1} so that

$$l_n \approx 20 \text{ m} < \min(l_\nu) = \left(\frac{\tilde{k}U_0}{\nu D}\right)^{-1/3} = 60 \text{ m}.$$

The critical level is thus controlled by dissipative processes and the linear approximation is justified. This discussion is based on our knowledge of steady critical levels. Nevertheless, in the unsteady case, the interaction may be different. It could be characterized by the unsteady scale, l_t,

$$l_t = \frac{1}{\tilde{k}\epsilon}\frac{\partial \epsilon}{\partial \tilde{t}} \Big/ \frac{d\tilde{u}_0}{\partial \tilde{z}} \approx \frac{D}{\tilde{k}U_0\tilde{t}_f} = 10 \text{ m} \leqslant l_\nu$$

(Churilov and Shukhman 1987), representing the distance to the critical level, above which the transience has important effects on the vertical structure of the wave. Because l_t is smaller than the viscous scale, the viscosity ensures that the critical-level interaction is quasi-steady.

Figure 11 represents the wave field at the times, $t = 6, 9, 12$ h for the three experiments. The vertical profiles of the incident flow and of the phase velocity are also drawn. At $\tilde{t} = 6$ h, the incident wind amplitude is maximal and the wave is still close to the ground (the wave amplitude is always zero above 15 km). This is due to the slow vertical propagation of the wave field

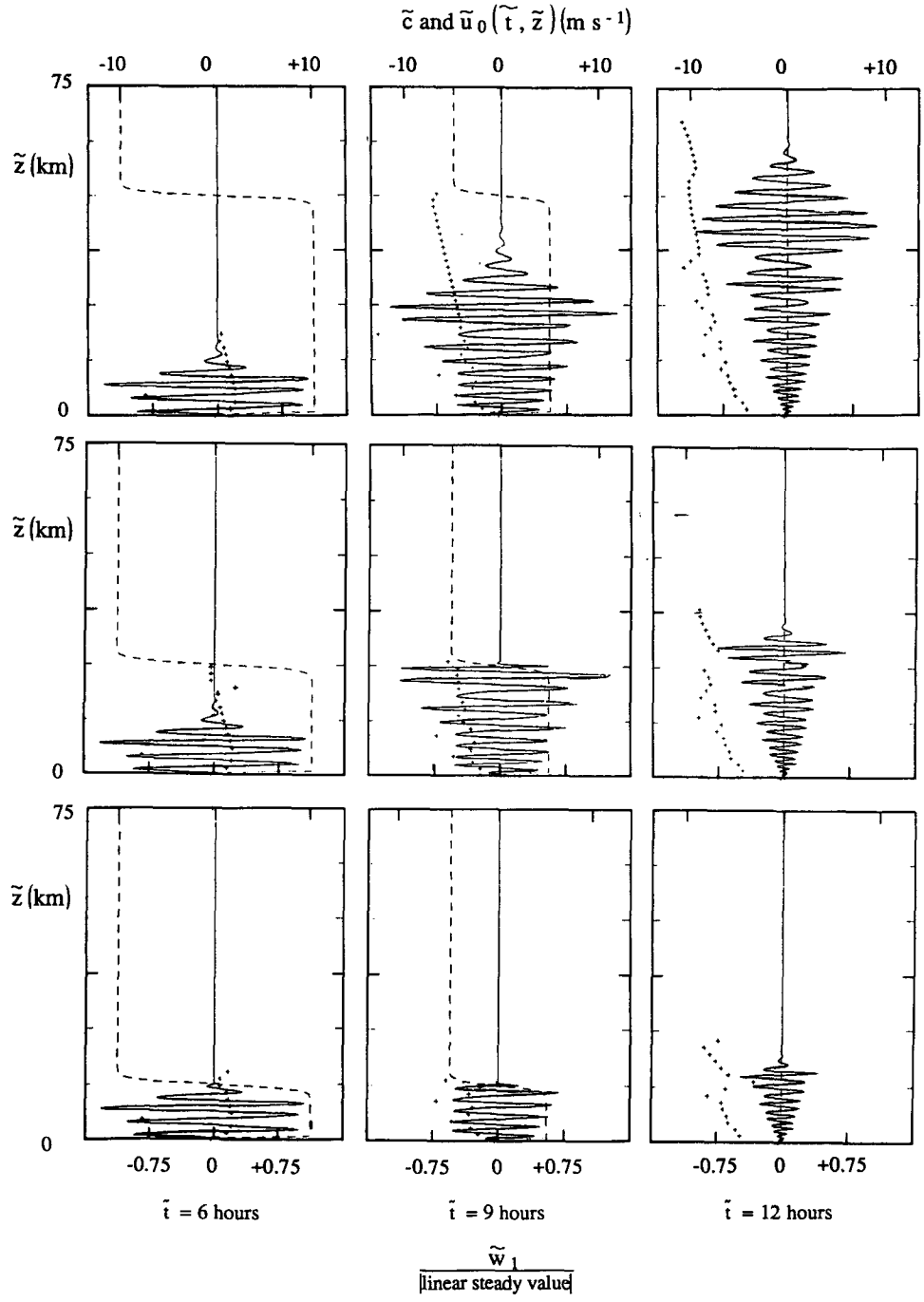

FIG. 11. Topographic waves generated by a vertically varying gust of wind. Top: $\tilde{z}_0$ = 50 km; middle: $\tilde{z}_0$ = 25 km; bottom: $\tilde{z}_0$ = 12.5 km, (solid) vertical velocity; (dash) mean wind; (plus signs) phase velocity. The temporal fluctuation of $\tilde{u}_0$ is given by (3.5), the vertical variation of $\tilde{u}_0$ is given by (3.7). Dimensional parameters: $\tilde{\lambda}_x$ = 13.1 km, H_0 = 10 m, U_0 = 10 m s^{-1}, N = 0.02 s^{-1}, $\tilde{t}_f$ = 6 h, ν = 1 m^2 s^{-1}.

during the increasing period of the incident wind. In fact, during this period, the waves present at the front have small amplitude intrinsic frequencies and propagate slowly compared to the maximum vertical group velocity, $(C_{gz})_{max}$ = 2.4 m s^{-1}. This behavior follows the discussion of the wave front propagation in section 2. As shown in Fig. 3, the caustic is initially tangent to the t axis, indicating a very slow vertical propagation

at the beginning of the wind. The front approaches the ray,

$$\tilde{z} = (\tilde{C}_{gz})_{\max}\tilde{t},$$

and propagates vertically at the maximum wave group velocity, after the moment of maximum incident wind. For this reason, the wave front reaches the shear layer only in the experiment for which $\tilde{z}_0 = 12.5$ km. The waves present at this time at the shear layer have almost zero phase velocity and encounter a critical level where they are absorbed. After this moment, the incident wind decreases and the phase velocities of the waves decrease similarly. The waves reaching the shear layer now have a negative phase velocity and can only encounter critical levels above $\tilde{z}_0$.

At $\tilde{t} = 9$ h and in the experiment for which $\tilde{z}_0 = 12.5$ km many waves have already encountered critical levels at the shear layer and have been absorbed. In the experiment for which $\tilde{z}_0 = 25$ km, the wave front has already reached the shear layer and some waves have been absorbed there. Nevertheless, at this moment, the waves arriving at the shear layer have phase velocities almost equal to the minimum wind. After this moment, they will no longer encounter critical level since their phase velocity will continue to decrease. In the experiment for which $\tilde{z}_0 = 50$ km, the front is far below the shear layer and so no critical level occurs.

At the end of the wind, $\tilde{t} = 12$ h, and in the experiment for which $\tilde{z}_0 = 12.5$ km, most of the waves have been absorbed at the shear layer and only residual gravity waves continue to propagate vertically. In the experiment for which $\tilde{z}_0 = 25$ km, the waves present in the frontal bulge have been absorbed at the critical level, and the others continue to propagate vertically. In the experiment for which $\tilde{z}_0 = 50$ km, the wave field is close to the one existing without the shear layer because the front reaches $\tilde{z}_0$ after the wind stops.

In these experiments, the gravity waves pass the shear layer when it is very high. Nevertheless, as the time scale, $\tilde{t}_w$, decreases when the horizontal wavenumber increases, longer waves will propagate more easily above the shear layer, even when it is located near the ground. The unsteady shear layer acts as a filter favoring the propagation of long unsteady mountain waves toward the middle atmosphere. Furthermore, these results seem to contradict the laboratory experiments of Thorpe (1981), where ground-forced gravity waves are absorbed at an unsteady shear layer resembling the one used in this section. Nevertheless, according to the preceding discussion, this is normal since in Thorpe (1981), the time scale, $\tilde{t}_w$, is very small as compared to the time scale of the unsteady wind. This is related to the narrowness of the tube he used. For instance, in one of the experiments depicted in Thorpe (1981, Fig. 4), where the mean flow increases and decreases successively, $\tilde{t}_w \approx 4 \times 10^{-2}$ s, whereas the time scale of the mean flow variation is 10 s, no wave is observed above the shear layer.

4. Conclusions

We have studied the linear gravity waves generated when a time-varying wind blows over a single harmonic mountain. The wave equations were first solved when the mean flow is uniform in the vertical direction and assuming the Boussinesq and hydrostatic approximations. By transforming the wave equations, the advection terms are simplified and it is possible to give an analytical form of the solution. When the incident wind is slowly varying (or quasi steady), an asymptotic form of the wave field is calculated using steepest descent methods. A time-dependent linear two-dimensional model is used when the mean flow varies rapidly, or when the mean wind also varies in the vertical direction.

If the mean flow is uniform in the vertical direction, it is found that the front of the wave field after the wind stops is nearly located along the line:

$$\tilde{z} = \tilde{k}U_0^2/N_0\tilde{t},$$

in the $(\tilde{z}, \tilde{t})$ plane. Here, $\tilde{t} = 0$ corresponds to the time at which the mean wind reaches its maximum value U_0, N_0 is the stratification, and $\tilde{k}$ is the horizontal wavenumber of the corrugated mountain. Above the front, the amplitude of the wave decreases to zero. Below it, it is a succession of bulges and nodes. Their number increases when the duration of the wind increases. The maximum amplitude attained in each bulge at a given time increases with $\tilde{z}$. It is at its maximum at the frontal bulge. When the wind stops, the phase velocity of the wave field varies from 0 at the ground to less than $-U_0$ above the wave front.

When the mean flow is quasi-steady, it is possible to identify this solution as the superposition of mountain gravity wave packets generated when the wind blows. It is found that these wave packets propagate along straight rays in the $(\tilde{z}, \tilde{t})$ plane. The wave front is then defined as the caustic of these rays. During their propagation, each of these packets conserves its relative phase velocity and its vertical wavenumber. Furthermore, the wave amplitude is maximum at the wave front because the waves that arrive here were generated at the ground when the mean wind was at its maximum. These waves also have the largest vertical group velocity since they have the smallest (negative) intrinsic frequency. The final form of the wave field below the front results from the interference between the group of waves generated while the incident wind increases, and the group of waves generated when it decreases. Furthermore, during the increasing phase of the wind, all the waves tend to propagate leeward the mountain. After the wind stops, all the waves propagate windward the mountain. In fact, the (negative) relative horizontal

group velocity of a given wave packet, which is opposite to the wind when it is generated, is no longer balanced by the advection when the wind ceases.

These results can have important consequences on the dynamics of the atmosphere. Because the wave field is transient, topographic waves tend to alter the mean flow during their propagation. At a given height, it is found that the mean flow is successively decelerated and accelerated at the passage of each bulge. Furthermore, the maximum amplitude of the momentum flux decreases in time because the wave field is very dispersive. These oscillations are also found when the transient incident wind is asymmetric (i.e., the duration of the decreasing period of the flow differs from its increasing period) or when it reaches a constant value. This behavior is very different from that of a wave field forced by a corrugated source whose amplitude varies while its phase velocity stays constant. In the latter case, the resulting wave field is not dispersive, the maximum amplitude of the momentum flux is constant, and no oscillation of the mean flow occurs. This indicates that some classical results (Dunkerton 1981; Dunkerton and Fritts 1984) concerning the transient gravity wave–mean flow interaction in the middle atmosphere do not apply when gravity waves are forced by topography. This also shows that it is not the same to start a numerical model of topographic waves by increasing the height of a mountain in a constant wind as to start it by increasing the amplitude of the incident flow.

The fact that mountain waves can be unsteady has other important consequences on their interaction with the background flow. This is particularly evident when they propagate through a zero wind level. This problem has been studied when the mean flow always reverses direction at a given height. Then, the wave–mean shear interaction depends mainly on the relative size of $\tilde{t}_w$, the minimum time required for a wave packet generated at the ground to reach the shear layer, and of $\tilde{t}_f$, which characterizes the temporal fluctuation of the mean flow. When $\tilde{t}_w < \tilde{t}_f$, many waves reach the shear layer when the shear intensity is still large, and are absorbed at critical levels. This corresponds to the configuration studied in Thorpe (1981) and explains why he did not observe transmitted waves above the shear layer. When $\tilde{t}_w > \tilde{t}_f$, the wave front has not attained the shear layer when the wind stops and no critical-level interaction occurs. The wave pattern is close to the one found when the mean flow is uniform in the vertical direction. In this case, there is an important flux of energy and momentum propagating above the shear layer, and the waves propagate toward high atmospheric levels. In a study of the propagation of mountain waves toward the stratosphere and mesosphere, Schoeberl (1987) found that mountain waves are able to propagate toward these levels in the steady case because the mean wind does not go to zero. In the present study, the unsteadiness allows the mountain waves to propagate toward high levels in spite of the existence of zero-level winds. This study also shows that unsteady gravity waves, often observed in the middle atmosphere (for instance, see Ebel et al. 1987), can be mountain waves.

These results also have implications for the current gravity-wave parameterization schemes used in general circulation models (Palmer et al. 1986) and suggest that such schemes estimate crudely the trajectories and the phase velocity of mountain waves. This study further shows that the unsteady structure of the wave field can be described using (time-varying) ray-tracing techniques. This could provide a basis for the improvement of these schemes including nonstationary effects. Nevertheless, additional studies have to be made to get a better comprehension of the incidence of these unsteady effects on the mountain waves. For this purpose, this type of work has to be extended to more realistic mountain profiles, to more realistic vertical wind profile, and to more rapidly fluctuating winds. It would also be essential to study the incidence of nonstationary effects on the location of the wave-breaking zones.

REFERENCES

Andrews, D. G., and M. E. McIntyre, 1976: Planetary waves in horizontal and vertical shear: The generalized Eliassen–Palm relation and the mean zonal acceleration. *J. Atmos. Sci.*, **33,** 2031–2048.

Bacmeister, J. T., and R. T. Pierrehumbert, 1988: On high drag states of nonlinear stratified flow over an obstacle. *J. Atmos. Sci.*, **45,** 63–80.

——, and M. R. Schoeberl, 1989: Breakdown of vertically propagating two-dimensional gravity waves forced by orography. *J. Atmos. Sci.*, **46,** 2109–2134.

Bannon, P. R., and J. A. Zehnder, 1985: Surface pressure and mountain drag for transient airflow over a mountain ridge. *J. Atmos. Sci.*, **42,** 2454–2462.

Bell, T. H., 1975: Lee waves in stratified flows with simple harmonic time dependence. *J. Fluid Mech.*, **67,** 705–722.

Booker, J. R., and F. B. Bretherton, 1967: The critical layer for internal gravity waves in a shear flow. *J. Fluid Mech.*, **27,** 513–539.

Brown, S. N., and K. Stewartson, 1980: On the nonlinear reflection of a gravity wave at a critical level, Part 1. *J. Fluid Mech.*, **100,** 577–595.

Chimonas, G., 1977: A possible source mechanism for mountain associated infrasound. *J. Atmos. Sci.*, **34,** 806–811.

Churilov, S. M., and I. G. Shukhman, 1987: Non linear stability of a stratified shear flow: A viscous critical layer. *J. Fluid Mech.*, **180,** 1–20.

Clark, T. L., and W. R. Peltier, 1984: Critical level reflection and the resonant growth of nonlinear mountain waves. *J. Atmos. Sci.*, **41,** 3122–3134.

Dunkerton, T. J., 1981: Wave transience in a compressible atmosphere. Part I: Transient internal wave, mean-flow interaction. *J. Atmos. Sci.*, **38,** 281–297.

——, and D. C. Fritts, 1984: The transient gravity wave critical layer. Part I: Convective adjustment and the mean zonal acceleration. *J. Atmos. Sci.*, **41,** 992–1007.

Durran, D. R., 1986: Another look at downslope windstorms. Part I: The development of analogs to supercritical flow in an infinitely deep, continuously stratified fluid. *J. Atmos. Sci.*, **43,** 2527–2543.

——, and J. B. Klemp, 1987: Another look at downslope winds. Part II: Nonlinear amplification beneath wave-overturning layers. *J. Atmos. Sci.*, **44,** 3402–3412.

Ebel, A., A. H. Manson, and C. E. Meek, 1987: Short period fluctuations of the horizontal wind measured in the upper middle atmosphere and possible relationships to internal gravity waves. *J. Atmos. Terr. Phys.*, **49,** 385–401.

Eliassen, A., and E. Palm, 1960: On the transfer of energy in stationary mountain waves. *Geophys. Norv.*, **22**(3), 1–23.

Fritts, C. J., and T. J. Dunkerton, 1984: A quasi linear study of gravity wave saturation and self acceleration. *J. Atmos. Sci.*, **41,** 3272–3288.

Grimshaw, R., 1975: Nonlinear internal gravity waves and their interaction with the mean wind. *J. Atmos. Sci.*, **32,** 1779–1793.

Hazel, P., 1967: The effect of viscosity and heat conduction on internal gravity waves at a critical level. *J. Fluid Mech.*, **30,** 775–783.

Jones, W. L., 1968: Reflection and stability of waves in stably stratified fluid with shear flow: A numerical study. *J. Fluid Mech.*, **34,** 609–624.

Jusem, J. C., and A. Barcilon, 1985: Simulation of moist, mountain waves with an anelastic model. *Geophys. Astrophys. Fluid Dyn.*, **33,** 259–276.

Klemp, L. B., and D. K. Lilly, 1975: The dynamics of wave-induced downslope winds. *J. Atmos. Sci.*, **32,** 320–339.

Landau, L. D., and E. M. Lifshitz, 1959: *Fluid Mechanics.* Pergammon Press.

Laprise, R., and W. R. Peltier, 1989: The structure and energetics of transient eddies in a numerical simulation of breaking mountain waves. *J. Atmos. Sci.*, **46,** 565–585.

Lightill, M. J., 1978: *Waves in Fluids.* Cambridge University Press.

Lindzen, R. S., 1981: Turbulence and stress due to gravity wave and tidal breakdown. *J. Geophys. Res.*, **86,** 9707–9714.

——, and K. K. Tung, 1978: Wave overreflection and shear instability. *J. Atmos. Sci.*, **35,** 1626–1632.

——, and A. J. Rosenthal, 1983: Instabilities in a stratified fluid having one critical level. Part III: Kelvin Helmholtz instabilities as over-reflected waves. *J. Atmos. Sci.*, **40,** 530–542.

——, and J. W. Barker, 1985: Instability and wave overreflection in stably stratified shear flow. *J. Fluid Mech.*, **151,** 189–217.

——, and S. R. Rambaldi, 1986: A study of over-reflection in viscous Poiseuille flow. *J. Fluid Mech.*, **165,** 355–372.

Long, R. R., 1953: Some aspects of the flow of stratified fluids. I. A theoretical investigation. *Tellus,* **5,** 42–58.

Lott, F., and H. Teitelbaum, 1990: Influence of dissipation on gravity waves propagating through a shear layer and on instabilities: validity of the linear approximation. *Ann. Geophys.*, **8**(1), 37–52.

Palm, E., 1953: On the formation of surface waves in a fluid flowing over a corrugated bed and on the development of mountain waves. *Astroph. Norv.*, **5**(3).

Palmer, T. N., G. J. Shutts, and R. Swinbank, 1986: Alleviation of a systematic westerly bias in general circulation and weather prediction models through an orographic gravity wave drag parameterization. *Quart. J. Roy. Meteor. Soc.*, **112,** 1001–1039.

Peltier, W. R., and T. L. Clark, 1979: The evolution and stability of finite-amplitude mountain waves. Part II: Surface drag and severe downslope windstorms. *J. Atmos. Sci.*, **36,** 1498–1529.

Queney, P., 1947: Theory of perturbations in stratified currents with application to airflow over mountains. Misc. Report No 23, University of Chicago Press, 81 pp.

Schoeberl, M. R., 1985: The penetration of mountain waves into the middle atmosphere. *J. Atmos. Sci.*, **42,** 2856–2864.

——, 1988: A model of stationary gravity wave breakdown with convective adjustment. *J. Atmos. Sci.*, **45,** 980–992.

Scorer, R. S., 1949: Theory of waves in the lee of mountains. *Quart. J. Roy. Meteor. Soc.*, **75,** 41–56.

Smith, B. S., 1979: The influence of the earth's rotation on mountain wave drag. *J. Atmos. Sci.*, **36,** 177–180.

——, 1982: Synoptic observations and theory of orographically disturbed wind and pressure. *J. Atmos. Sci.*, **39,** 60–70.

——, 1984: A theory of lee cyclogenesis. *J. Atmos. Sci.*, **41,** 1159–1168.

Thorpe, S. A., 1981: An experimental study of critical layers. *J. Fluid Mech.*, **103,** 321–344.